Biophysical Journal Volume 68 May 1995 2081–2090

Simulation of the S_2 State Multiline Electron Paramagnetic Resonance Signal of Photosystem II: A Multifrequency Approach

Karin A. Åhrling*‡ and R.J. Pace*

*Department of Chemistry, Australian National University, Canberra 0200; and ‡Cooperative Research Center for Plant Science, Canberra, 2601, Australia

ABSTRACT The S_2 state electron paramagnetic resonance (EPR) multiline signal of Photosystem II has been simulated at Q-band (35 Ghz), X-band (9 GHz) and S-band (4 GHz) frequencies. The model used for the simulation assumes that the signal arises from an essentially magnetically isolated Mn^{III}–Mn^{IV} dimer, with a ground state electronic spin $S_T = 1/2$. The spectra are generated from exact numerical solution of a general spin Hamiltonian containing anisotropic hyperfine and quadrupolar interactions at both Mn nuclei. The features that distinguish the multiline from the EPR spectra of model manganese dimer complexes (additional width of the spectrum (195 mT), additional peaks (22), internal "superhyperfine" structure) are plausibly explained assuming an unusual ligand geometry at both Mn nuclei, giving rise to normally forbidden transitions from quadrupole interactions as well as hyperfine anisotropy. The fitted parameters indicate that the hyperfine and quadrupole interactions arise from Mn ions in low symmetry environments, corresponding approximately to the removal of one ligand from an octahedral geometry in both cases. For a quadrupole interaction of the magnitude indicated here to be present, the Mn^{III} ion must be 5-coordinate and the Mn^{IV} 5-coordinate or possibly have a sixth, weakly bound ligand. The hyperfine parameters indicate a quasi-axial anisotropy at Mn^{III}, which while consistent with Jahn-Teller distortion as expected for a d^4 ion, corresponds here to the unpaired spin being in the ligand deficient, z direction of the molecular reference axis. The fitted parameters for Mn^{IV} are very unusual, showing a high degree of anisotropy not expected in a d^3 ion. This degree of anisotropy could be qualitatively accounted for by a histidine ligand providing π backbonding into the metal d_{xy} orbital, together with a weakly bound or absent ligand in the x direction.

INTRODUCTION

The Oxygen Evolving Center (OEC) of Photosystem II (PSII) catalyzes the oxidation of water to molecular oxygen. The OEC contains four manganese ions, and water molecules are known to be associated with this Mn cluster (Hansson et al., 1986). A photon of light causes the oxidation of the PSII reaction center chlorophyll a molecule (P680). The reaction center is subsequently reduced by an electron from the OEC. The total energy necessary to split water is accumulated in a four-step process, each electron removed resulting in an intermediate oxidation state of the OEC, the so-called S-states, labeled S_0–S_4. (Kok et al., 1970). Molecular oxygen is released after the fourth electron is removed, in the S_4 state, and the cycle repeats. In the dark, the OEC relaxes to the S_1 state. Continuous illumination of PSII particles in the S_1 state at 200 K generates the S_2 state without further advancement.

The S_2 state is paramagnetic and gives rise to two characteristic electron paramagnetic resonance (EPR) signals, a Mn hyperfine structured signal (the "multiline") centered around $g = 2$, and a broad, unresolved signal centered around $g = 4$ (the "4.1 signal"). Temperature dependence studies of these EPR signals are consistent with the multiline signal arising from an S = ½ ground state (Pace et al., 1991). An estimate of the antiferromagnetic exchange coupling (J) of the multiline signal in the presence of alcohol (~4% to the PSII sample buffer) gives $|J| > 10\ cm^{-1}$ (Pace et al., 1991). Britt and coworkers have confirmed that the multiline signal arises from a ground spin state (Britt et al., 1992; Lorigan and Britt, 1994), and this conclusion is now accepted. For a general overview see reviews by Debus (1992) and Hansson and Wydrzynski (1990).

Based on comparisons with model compounds (Dismukes and Siderer, 1981) and x-ray K-shell absorption studies (Goodin et al., 1984) the OEC is thought to consist of a pair of di-μ-oxo bridged Mn dimers organized in an as-yet-undetermined geometry. It is generally accepted that in the S_2 state, one pair of Mn ions differ in oxidation state by one (e.g., Mn^{III}-Mn^{IV}) and are antiferromagnetically coupled, yielding a net spin of ½. The other pair is assumed to be Mn^{III}-Mn^{III} or Mn^{IV}-Mn^{IV}, yielding a net spin of 0. Suitably weak interactions between the two pairs yield a system with spin ½ ground state (Liang et al., 1994).

Comparison of the multiline signal with X-band (~9 GHz) EPR spectra of dimeric model compounds reveals that the the multiline signal is more complex: it exhibits detailed internal "superhyperfine" structure and more than the 16 peaks generally observed in model compounds. Of particular note are the peaks of low, variable intensity beyond the commonly recognized width of ~180 mT (>18–20 peaks). The multiline Q-band (~35 GHz) spectrum shows the same number of peaks (Smith et al., 1993), but less of the superhyperfine structure, reflecting both linewidth effects and the increasing dominance of the Zeeman interaction at high microwave frequency. At lower frequencies, such as S-band (~4 GHz), the

Received for publication 30 December 1994 and in final form 24 February 1995.

Address reprint requests to Dr. R. J. Pace, Chemistry Department, Faculty of Science, Australian National University, G.P.O. Box 4, Canberra 0200, Australia. Tel.: 61-6-2494546; Fax: 61-6-2490760; E-mail: kaa651@cscgpo.anu.edu.au.

0006-3495/95/05/2081/10 $2.00

hyperfine interactions are relatively more important. The multiline spectrum at S-band is particularly complex, exhibiting ~50 lines. The resolved superhyperfine structure of the multiline signal cannot be attributed to ligand hyperfine interactions with protons or nitrogen from the protein matrix, nor with chloride that may be associated with oxygen evolution (DeRose et al., 1991; Yachandra et al., 1986; Andreasson, 1989; Haddy et al., 1989). Individual ligand hyperfine interactions of protons, nitrogen, or chloride with the metal cluster are narrower than the observed linewidth and are not usually resolved. Combined ligand hyperfine interactions, however, may contribute to the greater linewidth seen in the multiline signal, and in signals from metal clusters in proteins generally, compared with model compounds (Brudvig, 1989).

Haddy et al. (1994) have studied the EPR spectra of Mn^{III}-Mn^{IV} catalase at three frequencies (S-band, X-band, and P-band, ~15 GHz). Like model compounds, the catalase spectrum shows 16 peaks at X-band. The S-band spectrum (~20 peaks) does not exhibit the same complexity as the S-band of the PSII multiline signal. In fact, it is remarkably similar to the spectra at both X- and P-band. The additional complexity of the PSII S-band multiline signal, however, cannot be explained simply by a linewidth effect, nor can it be adequately explained in terms of hyperfine anisotropy alone.

The above factors have led to the belief that all four Mn ions give rise to the multiline pattern, with each Mn ion contributing substantially different effective hyperfine interactions to the total net spin = ½ system. Simulations based on the above assumption have appeared (Bonvoisin et al., 1992; Kusonoki, 1992; Zheng and Dismukes, 1992). The simulations, with the exception of those by Kusonoki et al., have been performed at X-band only, and no attempt has yet been made to address the superhyperfine structure or additional peaks. Even though oriented spectra at X-band (Rutherford, 1985) and S-band (Haddy et al., 1989) have shown that substantial hyperfine anisotropy exists in the center giving rise to the multiline signal, the simulations have been confined to isotropic (Bonvoisin et al., 1992; Kusonoki, 1992) or axial hyperfine parameters (Zheng et al., 1994).

Synthetic complexes of multimeric Mn have been prepared that attempt to model aspects of the structural organization and EPR properties of the OEC (e.g., Bashkin et al., 1987; Kessissoglou et al., 1989; Sarneski et al., 1990). Although all three model compounds have EPR signals that exhibit a ground S = ½ state signal with multiple lines, the only spectrum that resembles the OEC multiline signal (Kessissoglou et al., 1989) stems from a Mn^{III}-Mn^{II}-Mn^{III} trimer, whereas extended x-ray absorption fine structure (EXAFS) and x-ray absorption near edge spectroscopy studies indicate an average oxidation state greater than III for Mn in the S_2 state of the OEC (Goodin et al., 1984; Yachandra et al., 1987; Penner-Hahn et al., 1990).

EXAFS studies (MacLachlan et al., 1992; George et al., 1989; DeRose et al., 1994; Penner-Hahn et al., 1990) identify two Mn-metal interactions, one at 2.7 Å, one at 3.3–3.7 Å. The data indicate that the PSII Mn ions each have one Mn neighbor at a distance of 2.7 Å. There is general agreement that the scatterer at 3.3–3.7 Å results from one Mn-metal interaction (~0.5 neighbor/Mn). Depending on analysis, this could represent Mn-Mn or Mn-Ca and could also include interactions from carbon, oxygen, and nitrogen. Based on the above arguments, Klein and coworkers (Yachandra et al., 1993) favor a model of a pair of di-μ-oxo bridged dimers, linked by one μ-carboxylato bridge between one Mn ion of each pair. However, the EXAFS data are also consistent with two non-interacting pairs of Mn dimers, with a Ca ion associated with one of them. The data are not consistent with a trimeric cluster and a single isolated Mn ion within the OEC.

Parallel polarization EPR studies on the S_1 state of PSII (Dexheimer and Klein, 1992) show that the species that gives rise to the S_1 state signal converts only to the multiline signal in the S_2 state. The authors conclude that the two S_2 state signals (multiline and 4.1) originate from magnetically distinct centers within the OEC and therefore imply a model of non-interacting dimers. This conclusion is supported by recent work in this laboratory, suggesting that the four Mn ions are organized as two magnetically isolated, antiferromagnetically coupled pairs. Under appropriate conditions (in the presence of alcohol), one pair is EPR silent and the other gives a net S = ½ ground state (P. Smith and R. J. Pace, submitted for publication). For the Mn^{III}-Mn^{IV} pair to be magnetically isolated it needs to be physically isolated (but presumably within electron transfer distance, ~10 Å) or weakly coupled to a pair with net zero spin.

Zheng et al. (1994) have studied the factors that influence the number of resolved lines in the EPR spectra of Mn dimers. They found that the number of lines in the EPR spectrum of a Mn dimer differing in oxidation state by one and antiferromagnetically coupled, depends on the strength of the exchange interaction, which in turn directs the influence of the zero field splitting interaction on the spectrum. In particular, the number of lines can differ from 16 depending on the strength of these interactions.

The results summarized above indicate that the multiline signal in the S_2 state of PSII could arise from a magnetically isolated Mn^{III}-Mn^{IV} dimer. Here we explore circumstances under which such a dimer might give rise to the detailed multiline EPR spectrum observed in PSII. The large number of peaks resolved in the S-band multiline spectrum require that normally forbidden transitions have become substantially allowed. The most likely mechanism that could give rise to these normally forbidden transitions is one in which the two Mn centers in the protein have sufficiently low ligand symmetry so that Mn nuclear quadrupolar effects contribute significantly to the hyperfine interaction. Under such circumstances perturbation theory is inadequate to treat the spin Hamiltonian, and the problem must be solved numerically. The results reported here attempt to explain not only the general features of the multiline signal, but also its superhyperfine structure. Simulations were performed at three frequencies: S-band, X-band, and Q-band, for which good

experimental data are currently available. A brief discussion of possible ligand geometries for the dimer, consistent with the fitted parameter set is also given.

MATERIALS AND METHODS

Experimental procedures

PSII samples were prepared from greenhouse-grown spinach as previously described (Pace et al., 1991). The samples showed an activity of 500–600 mmol O_2/mg chlorophyll (chl) h^{-1}. The PSII samples were suspended at about 15 mg chl ml^{-1} in a buffer containing 20 mM 2-(*N*-morpholino)-ethanesulfonic acid (ph 6.0 KOH), 10 mM $MgCl_2$, 15 mM NaCl, and 400 mM sucrose. 4% ethanol and EDTA (1 mM) were added before illumination. The samples were allowed to adapt in the dark at room temperature for 10 min before illumination. For X-band measurements the samples were illuminated with green light for 4 min at 200 K, with subsequent storage at 77 K. The light intensity was 140 W m^{-2}. The X-band spectra have been reported earlier (Smith et al., 1993). Samples for Q-band spectra were prepared similarly but illuminated for 3 min at 220 K.

EPR measurements were performed on a Varian (Palo Alto, CA) V-4502 spectrometer equipped with an Oxford* ESR9 helium-flow cryostat (Oxford Instruments, Witney, UK) as described previously (Pace et al., 1991). Q-band measurements were performed on the same spectrometer using a homebuilt He flow cylindrical Q-band cavity, adapted from a Varian design (V4566) (R. Bramley, unpublished information). This was totally contained within an Oxford Instrument flow cryostat.

Theory and calculations

The magnetic exchange interaction Hamiltonian is taken to be $-2J\mathbf{S}_1 \cdot \mathbf{S}_2$, where J is the exchange interaction parameter between the two Mn centers (Abragam and Bleaney, 1986). From the temperature dependence of the signal intensity in the presence of ethanol, it is inferred that the multiline signal arises from a well-isolated ground state (gap to the nearest state >30 cm^{-1} (Pace et al., 1991)). The magnitude of the exchange interaction places the dimer in the strong coupling regime ($D/J \ll 1$, where D is a single ion zero-field splitting parameter), so that the exchange interaction spin states can be taken as the zeroth order states. For an antiferromagnetically coupled pair the total spin will take the following values: $S_T = \{1/2,3/2...7/2\}$, where $S_T = ½$ is the ground state for a dimer with a total spin 7/2 (Mn^{III}-Mn^{IV}).

The effective spin Hamiltonian for the system in a particular total spin state may be written as

$$\mathcal{H} = \mathbf{S}\cdot\mathbf{D}\cdot\mathbf{S} + \beta\mathbf{H}_o\cdot\mathbf{g}\cdot\mathbf{S} - \sum_{\text{nuclei}} (g_n\beta_n\mathbf{H}_o\cdot\mathbf{I} + \mathbf{I}\cdot\mathbf{A}\cdot\mathbf{S} + \mathbf{I}\cdot\mathbf{Q}\cdot\mathbf{I})$$

The fine structure interaction ($S \cdot D \cdot S$) does not contribute to the splitting for an S = 1/2 state. Considering only Mn hyperfine interactions, the simplified Hamiltonian takes this form:

$$\mathcal{H} = \beta\mathbf{H}_o\cdot\mathbf{g}\cdot\mathbf{S} - g_n\beta_n\mathbf{H}_o\cdot\mathbf{I}_1 - g_n\beta_n\mathbf{H}_o\cdot\mathbf{I}_2 + \mathbf{I}_1\cdot\mathbf{A}_1\cdot\mathbf{S}_T + \mathbf{I}_1\cdot\mathbf{Q}_1\cdot\mathbf{I}_1 + \mathbf{I}_2\cdot\mathbf{A}_2\cdot\mathbf{S}_T + \mathbf{I}_2\cdot\mathbf{Q}_2\cdot\mathbf{I}_2$$

Here $\mathbf{H}_o$ is the applied magnetic field vector, $\mathbf{g}$ the g-tensor, β the Bohr magneton, g_n the nuclear g value (assumed scalar), and β_n the nuclear Bohr magneton. The subscripts 1 and 2 refer to the Mn^{III} and Mn^{IV}, respectively.

$\mathbf{A}_1$ and $\mathbf{A}_2$ are the effective nuclear hyperfine interaction tensors including the spin projection factors for each individual ion spin. In the strong coupling limit, this gives $A_{1\text{effective}}$ (Mn^{III}) = $2a_1$ and $A_{2\text{ effective}}$ (Mn^{IV}) = $-a_2$ (Sands and Dunham, 1975), where a_1 and a_2 are the true ion parameters. Any contribution of the zero-field splitting term of the individual Mn ions (Zheng et al., 1994) to the hyperfine interaction is included in the effective hyperfine parameter A. $\mathbf{Q}_1$ and $\mathbf{Q}_2$ are the quadrupole interaction tensors, and $\mathbf{I}_1$ and $\mathbf{I}_2$ are the nuclear spin vectors (I = 5/2).

The applied magnetic field is taken to be along the laboratory z axis and expanding the Hamiltonian in the laboratory frame yields the expression given in Appendix I.

The principal axis systems for all tensors are assumed to be coincident, as a first approximation. Introducing non-coincident tensors would add many more variables and make the already extensive calculations prohibitive. In this system, where the tensors are assumed to be coincident, the field $\mathbf{H}_o$ makes polar angles θ, ϕ with the molecular (principal axis) frame. Any diagonal (molecular frame) matrix, $\mathbf{B}'$, can be transformed into the laboratory frame matrix $\mathbf{B}$ by a unitary transformation of the form $\mathbf{B} = \mathbf{R}\cdot\mathbf{B}'\cdot\mathbf{R}^{\dagger}$, where $\mathbf{R}$ is the matrix of direction cosines (see Appendix II).

The product spin functions $|m_{I1},m_{I2},m_s\rangle$ are taken as the basis functions for the Hamiltonian matrix (m_{I1},m_{I2} = + 5/2,...−5/2;m_s = −1/2,+1/2). The Hamiltonian matrix, $\langle m_s,m_{I2},m_{I1}|\,H\,|m_{I1},m_{I2},m_s\rangle$, generated in this way is 72 × 72 in size. The Hamiltonian is divided throughout by $g_{iso}\beta$, thereby generating energy levels in field units (Tesla, T). g_{iso} is the isotropic component of the g-tensor (⅓ the trace).

The matrix is diagonalized using a standard routine (NAG FO2AXF, The Numerical Algorithms Group Ltd, Oxford, UK) and the energy levels derived directly from the eigenvalues. In the field range of the resulting X- and Q-band spectra, the energy levels vary linearly with the field to a good approximation, and hence the field position where the transition occurs can be found by simple extrapolation (see Fig. 1). The linear relationship breaks down at lower frequencies. At S-band this is overcome by dividing the field range into three sections, over which range the field again can be considered linear, and calculating the spectrum in three sections.

The experimental multiline spectra are powder pattern spectra. Therefore, a number of random angles θ, ϕ as described above, that will suitably sample the random orientations of the molecule to the laboratory frame, have to be generated. For a system in which all tensor axes are coincident, it is sufficient to generate these angles over one octant of the unit sphere. The method chosen was to divide the surface of the octant into "tiles" of equal solid angle. To avoid biasing one edge of the octant an adjustment was made so that the average discrepancy in tiling was even along both meridians. A tile subtending an angle of 4.5°C along an edge results in 284 single crystal orientations added together to contribute to the powder pattern, which has been found to be more than adequate to reduce any sampling noise on the simulation (see Appendix III). A Gaussian envelope was centered on each individual transition, with the width parameter as the only lineshape variable. No dependence on m_I or orientation was included.

The EPR transition probability (I) is proportional to $|\langle m_{up}|\,\beta\mathbf{H}_1\cdot\mathbf{g}\cdot\mathbf{S}\,|m_{down}\rangle|^2$, where H_1 is the amplitude of the applied microwave field magnetic vector and $\langle m_{up}|$, $\langle m_{down}|$ are the states between which the transition occurs. For a conventional system with the applied field H_o along the z

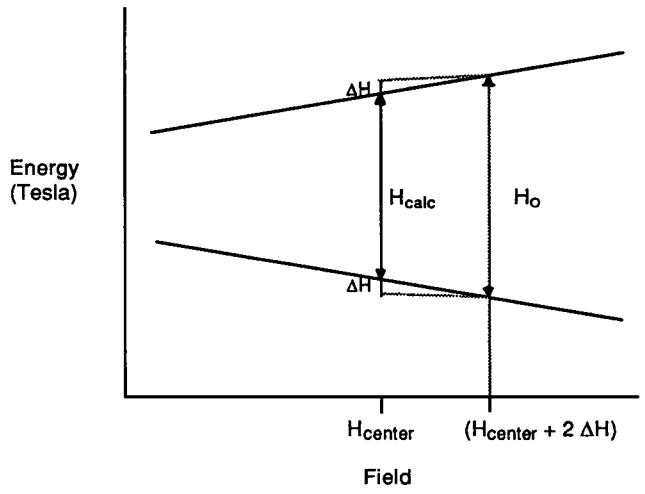

FIGURE 1 Field positions corresponding to particular transitions between pairs of states are calculated from the difference in eigenvalues of those states, H_{calc} (in field units). In the diagram, $2\Delta H = H_o - H_{calc}$, where H_o is the microwave quantum for the spectrum (in field units). Then the transition occurs at $H_{obs} = H_{center} + 2\Delta H = H_o + H_{center} - H_{calc}$, where H_{center} is the center field (calculation point) for the spectral region to be simulated.

direction and small g anisotropy (estimated at ±0.5% (Smith et al., 1993)), the simplified expression $I = \text{Const} |\langle m_{up}|S_x + S_y|m_{down}\rangle|^2$ is obtained. When the system has $S_T = 1/2$ it is sufficient to calculate $I = \text{Const} |\langle m_{up}|S_+|m_{down}\rangle|^2$, where S_+ is the raising operator. The derivative of the absorption spectrum was computed numerically for comparison with the experimental data.

Minimization of the fit was carried out using a simplex routine (AMOEBA; Press et al., 1986). This routine minimized

$$X^2 = \sum_{i=1}^{n} (Y_i^{sim} - Y_i^{exp})^2$$

where Y represents the amplitude of the derivative spectrum at a point of the field, and n is the number of field points. A minimum was reached when

$$\text{Tol} = 2\times |X^2_{high} - X^2_{low}|/(|X^2_{high}| - |X^2_{low}|)$$

was less than a predetermined tolerance, $\text{Tol} = 1 \times 10^{-4}$.

RESULTS AND DISCUSSION

Experimental spectra

The Q-band spectrum (Fig. 2, *A* and *B*) was acquired as the illuminated-minus-dark spectrum of the downfield (Fig. 2 *A*) and the upfield (Fig. 2 *B*) portions of the multiline signal, acquired on separate 100 mT scans. The spectrum is the average of 15 sets of scans. The break in the spectrum results from the removal of a superimposed radical signal at $g = 2$. The X-band spectrum (Fig. 3, *A* and *B*) seen here has been reported previously (Smith et al., 1993). The S-band spectrum (Fig. 4, *A* and *B*) is reproduced with permission (Haddy et al., 1989).

In addition to the main X-band spectrum, spectra of the edges of the multiline signal were carefully acquired to ascertain the width of the spectra. Other workers (Bonvoisin et al., 1992) have indicated peaks below 240 mT and above 410 mT in addition to those 18–20 peaks commonly observed. When simulating the superhyperfine structure, these additional peaks of varying low intensity become important. Variable frequency studies at X-band (R. J. Pace and P. Smith, unpublished data) have shown that peaks in addition to the ~22 peaks attributed to the multiline signal have an apparent g-value quite different from that of the multiline signal. These peaks have therefore not been included. The X-band spectrum of ~22 peaks gives an overall width differing from that reported by us previously (Smith et al., 1993). The spectral edge, as we now see it, corresponds closely to the width of the simulation (see Fig. 3, *A* and *B*).

Simulations

The simulated spectra are shown in Fig. 2–4 and the parameters used listed in Table 1. Fig. 5. Often the multiline spectra show an underlying broad signal centered around $g = 2$. The spectra from PSII preparations in the presence of ethanol (4%) as shown here have less of this broad signal than spectra from preparations without added alcohol (see Pace et al., 1991). The amount of this underlying signal is variable, and it appears to have a different temperature dependence from that of the multiline signal. Some of it is present in dark adapted samples, and some may be photoinduced (Pace et al., 1991). It is clear from S-band spectra (see Haddy et al., 1989) that the underlying signal is not merely a broadening due to increase in linewidth. Haddy et al. (1989) see very little underlying signal in the light-minus-dark spectrum of PSII-enriched membranes, whereas in spectra from core preparations the underlying signal is large. The source of the broad signal is not understood, but could perhaps be due to protein bound, inactive Mn. Antiferromagnetic coupling of dimers of the same oxidation state would lead to an $S = 0$ ground state, not visible by EPR, but the first excited state $S = 1$ would be present as a broad signal if significantly populated at the observation temperature. The underlying signal in the multiline spectrum could perhaps be due partially to centers in the S_1 state after illumination. Samples without alcohol, which are inferred to have a smaller antiferromagnetic coupling (at least in the S_2 state) (Pace et al., 1991) show more underlying signal, which supports this argument.

The underlying broad signal, as shown in Pace et al. (1991), has been subtracted from the experimental spectrum. Examination of the integrated experimental spectra (as seen in Fig. 6) is used to ensure a consistent subtraction of the (derivative) underlying signal. The total intensity is calculated by a double integration and used to scale the experimental spectrum to the simulated spectrum.

To simulate the spectra, the general procedure has been to start with a minimum number of parameters, incorporating additional interactions as required. Once an overall general fit has been achieved, by single calculations, the simplex routine was linked to the program. Initially only the major parameters were allowed to vary, gradually adding all parameters to vary in the minimization. The parameters were then swapped between X- and Q-band minimizations. In this fashion an overall fit was achieved. The S-band spectrum is

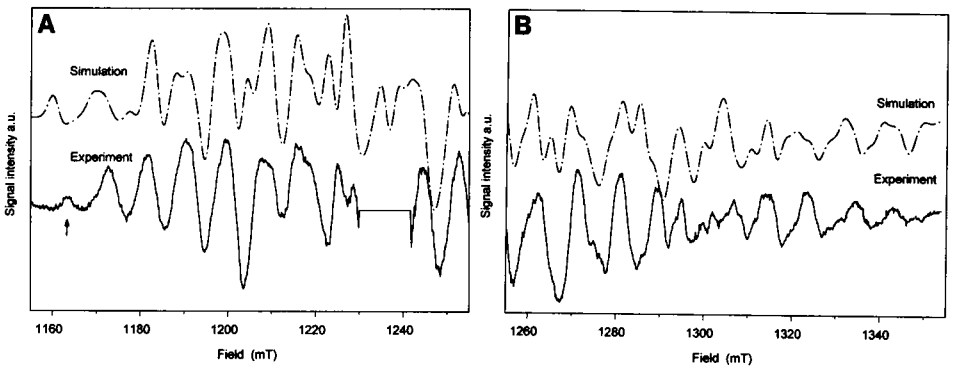

FIGURE 2 (*A* and *B*) Q-band simulated and experimental spectra, spectrometer conditions: frequency 34.64 GHz, 0.5 mT modulation amplitude, 30 mW microwave power, 100 kHz modulation frequency, temperature 8 K. Spectra are the averages of 15 scans, and the upfield and downfield regions were acquired on separate 100 mT scans. The parameters used in the simulation are listed in Table 1. Arrow here and in Fig. 3 *A* indicates lowest field peak that we unambiguously identify with multiline spectrum.

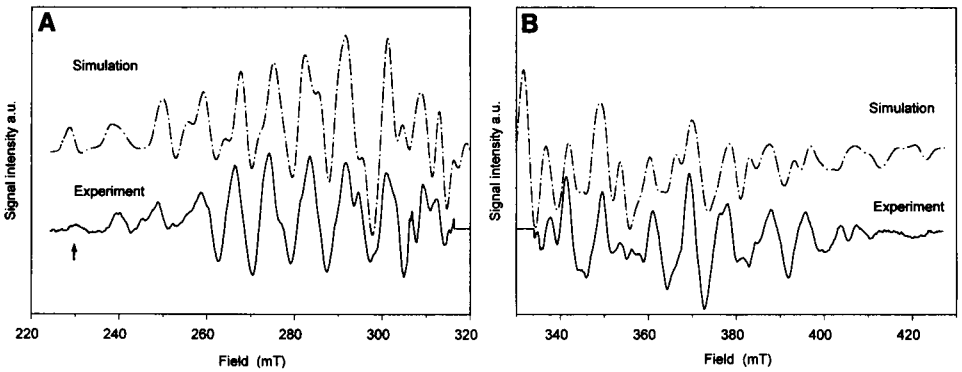

FIGURE 3 (*A* and *B*) X-band simulated spectrum and experimental spectrum as seen in Smith et al. (1993). Spectrometer conditions: frequency 9.04 GHz, 2 mT modulation amplitude, 30 mW microwave power, 100 kHz modulation frequency, temperature 8 K. Spectra are averages of five scans, and the upfield and downfield regions were acquired on separate 100 mT scans. The parameters used in the simulation are listed in Table 1.

much more complex, and minimization was only attempted at S-band when a good fit had been achieved at both X- and Q-band.

g-value

The values for g_x and g_y (~1.965 from Q-band) are lower than our earlier estimate of $g_\perp$~1.984 (Smith et al., 1993) and that found by Hansson et al. (1987) of $g = 1.982 \pm 0.002$. This difference is due to what we now believe to have been an alignment error of one peak spacing (i.e., ~9.0 mT) between the experimental X- and Q-band spectra, when estimating the apparent g-value. A correct alignment depends crucially on identifying the true edges of the spectra, particularly in the downfield region where the peaks are of more regular spacing. The lowest field peaks that we can now unambiguously identify with the experimental multiline spectra at X- and Q-band are indicated in Figs. 2 *A* and 3 *A*. Aligning from these gives an experimental estimated for g of 1.967. The value of g_z is more difficult to estimate as the z axis is contracted compared with the x and y axes for all other parameters. The minimization for the three frequencies has indicated a value near 2.00, but the error may be ±0.014.

Quadrupole interaction

The quadrupole interaction depends on the product of the nuclear quadrupole moment and the nonspherically symmetric component of the electric field gradient at the nucleus. The Mn nucleus is a good potential candidate as the nuclear quadrupole moment of ^{55}Mn is ~0.4, about 5 times larger (Landolt-Börnstein, 1988) in magnitude than that of ^{35}Cl (~ −0.08), which is routinely studied by quadrupole spectroscopy. The quadrupole interaction is not often seen by EPR in synthetic Mn complexes, because the Mn ligand environment is relatively symmetric, which gives an electric field gradient at the nucleus of the central cation that is nearly spherical. However, the ~50 lines seen in the S_2 state S-band spectrum, compared with the ~20 in the manganese catalase enzyme (Haddy et al., 1994), is an indication that the environment for the OEC may be highly strained, leading to large nuclear quadrupolar effects. For a quadrupole interaction of the magnitude seen here, the ligand distribution must be highly nonsymmetric, i.e., at least one ligand must be weakly bound (ionic or distant) or not be present at all. In addition, because the magnitude of the quadrupole interaction has a $\langle 1/r^3 \rangle$ dependency (Slichter, 1978), where r is the distance between the electron charge and the nucleus, the charge density must be close to the central cation to contribute significantly to the interaction, i.e., the ligands must be backbonding into vacant metal orbitals.

The quadrupole interaction at Mn^{III} is quasi-axial. The sign of the quadrupole interaction ($Q_\perp$ negative) indicates that the bonding is covalent. An attempt was made to fit a quadrupole interaction with $Q_\perp$ positive (i.e., the electric field gradient was dominated by Mn d orbital charge distribution), but no satisfactory composite fit could be achieved over the three frequencies. LCAO Xα calculations of magnetic exchange

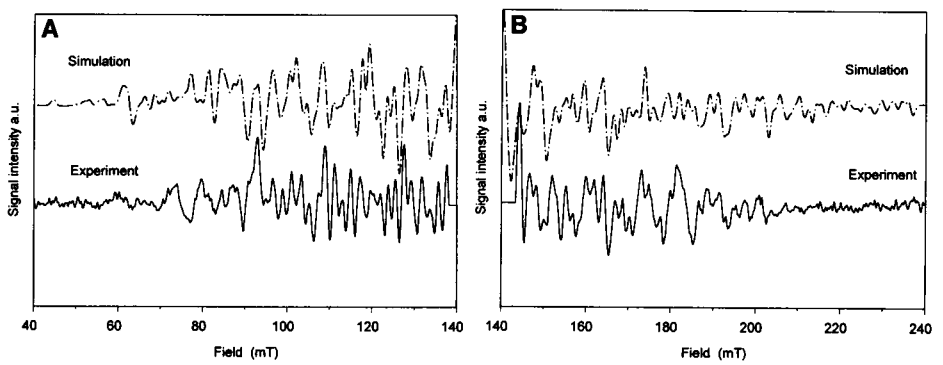

FIGURE 4 (*A* and *B*) S-band simulated spectrum and experimental spectrum as reported in (Haddy et al., 1989) reproduced with kind permission by the authors. Frequency 3.91 GHz. 2% ethanol and 100 mM 3-(3,4-dichlorophenyl)-1,1-dimethylurea added. The parameters used in the simulation are listed in Table 1.

TABLE 1 Fitted simulation parameters to the S_2 state EPR multiline signal of PSII at Q-, X- and S-band

Parameter* (mT)	Q-band	X-band	S-band
$a1_{iso}$‡	−8.4	−8.2	−8.0
$a2_{iso}$‡	−9.4	−9.2	−9.1
$a1x$	−9.8	−9.8	−9.7
$a1y$	−11.9	−11.6	−11.7
$a1z$	−3.4	−3.1	−2.6
$q1x$	−0.76	−0.76	−0.80
$q1y$	−1.00	−1.00	−1.11
$q1z$	+1.76	+1.76	+1.91
$a2x$	−9.8	−9.4	−9.1
$a2y$	−12.7	−13.1	−13.3
$a2z$	−5.8	−5.0	−5.0
$q2x$	+1.83	+1.83	+1.72
$q2y$	−0.96	−0.96	−0.91
$q2z$	−0.87	−0.87	−0.82
gx	1.9652	1.9716	1.9716
gy	1.9664	1.9739	1.9739
gz	1.9930	2.0092	2.0092
linewidth	1.8	1.6	0.8

*True single ion parameters assuming a coupled Mn^{III}-Mn^{IV} dimer with A_1 effective (Mn^{III}) = $2a_1$ and A_2 effective (Mn^{IV}) = $-a_2$ (Sands and Dunham, 1975).

‡$a1_{iso}$ = (a1x + a1y + a1z)/3.

interactions in a Mn^{IV}-Mn^{III}_3 cubane complex have been carried out (Schmitt et al., 1992). For both Mn^{III} and Mn^{IV} there was substantial mixing of metal and ligand atomic wave functions in the molecular orbitals (MOs). The calculation of overall charge at each Mn showed appreciable covalency in the bonding. The above suggests that the quadrupole interaction results from significant backbonding of σ bonding electron pairs from the ligands into vacant $3d$ (e_g orbitals) and $4p$ orbitals. The contribution is mainly in the xy plane, indicating that the ligands are concentrated in this plane. The z direction must be depleted of at least one ligand for such an interaction to be seen (see Fig. 7).

The interaction at Mn^{IV} is also quasi-axial but in this case about the x axis, indicating that the *net* charge density and therefore the ligands are concentrated in a plane containing the y and z axes. The interaction is similar in magnitude to

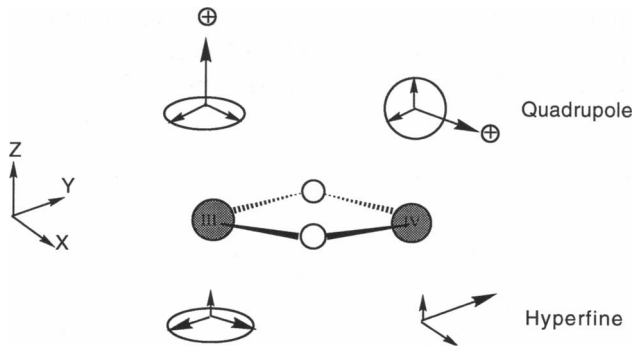

FIGURE 5 Orientation of the molecular axis together with the symmetry of the quadrupole and hyperfine interactions after minimization. The latter are represented symbolically in magnitude as shown. The assignment of the z axis as indicated is not certain, but is favored as it places the μ-oxo bridges in the xy plane. This is the most likely orientation for Mn^{III}, the hyperfine parameters of which are most easily interpreted structurally.

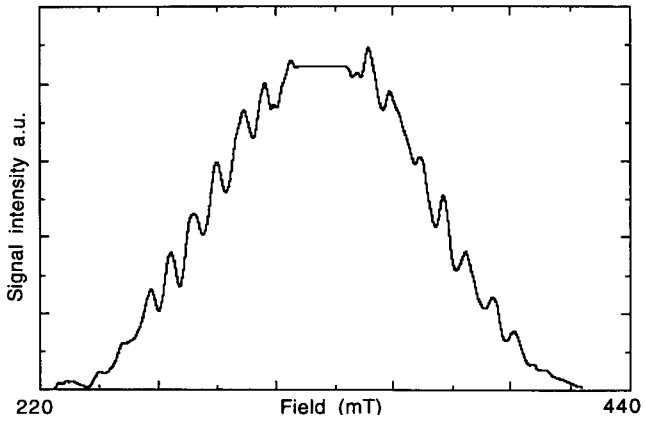

FIGURE 6 Integrated experimental X-band spectrum after the underlying broad signal has been subtracted from the derivative spectrum. The center section has been removed, as it contains a component from a tyrosine radical.

the quadrupole term for Mn^{III}. The x axis, from the above arguments, could only have one covalently bound ligand contributing to the charge density at the nucleus. The other ligand position could be occupied by a weakly bound ligand, or unoccupied.

The quadrupole interaction contributing to the multiline can be determined by a spin-echo or ENDOR experiment. Such experiments are currently in preparation in our laboratory.

Hyperfine interaction

Mn^{III} is a d^4 high spin ion and therefore has one of the e_g orbitals occupied. The hyperfine interaction at Mn^{III} is quasi-axial, consistent with the Jahn-Teller distortion expected for a d^4 ion. The d_{z^2} orbital is the e_g occupied, as evidenced by the smaller magnitude of the $a1z$ parameter relative to $a1x$,$a1y$, an observation also noted in the manganese catalase enzyme (Zheng et al., 1994; Haddy et al., 1994). The degree of axial anisotropy is substantially larger, however, for the Mn^{III} in the OEC. The isotropic hyperfine value, a_{iso}, for Mn^{III} of −8.4 mT is within the expected range (Al'tshuler and Kozyrev, 1974). The symmetry of the hyperfine interaction is consistent with that of the quadrupole interaction, together indicating that the highest energy orbital, $d_{x^2-y^2}$, is vacant of unpaired spin density, and the d_{z^2} orbital has only one ligand aligned with it.

The anisotropic hyperfine interaction at Mn^{IV} of the OEC is to our knowledge unprecedented. In considering whether such a value is reasonable we note that the hyperfine interactions of the Mn dimer must be unusual to give rise to the >20 line spectra, with superhyperfine structure that sets the multiline signal apart from other systems such as the manganese catalase and model compounds. The parameters indicate a substantial rhombic anisotropy not expected for a d^3 ion in a near-octahedral environment. The unpaired electron spin density resides mainly along the z direction, with the y direction most depleted of spin. This can be interpreted in terms of a substantially covalent π bonding interaction be-

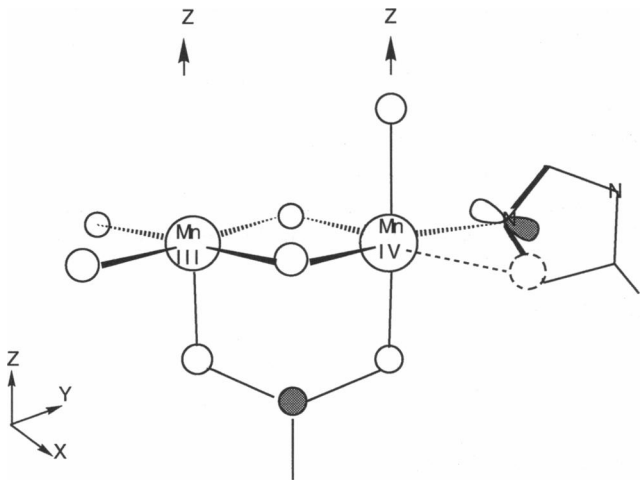

FIGURE 7 One interpretation of the parameter set given by the simulation. The Mn-dimer is di-μ-oxo, μ-carboxylato bridged. The histidine is liganded to the Mn^{IV}. The dashed circle indicates a distant or very weakly bound ligand. Mn^{III} is 5-coordinate.

tween the metal ion and the ligands in a low symmetry environment. The antibonding MOs arising from the three metal t_{2g} orbitals and ligand p orbitals will have different amounts of metal orbital character along the x, y, and z directions. Because of the $\langle 1/r^3 \rangle$ dependence of the dipolar hyperfine interaction (Abragam and Bleaney, 1986), only the metal d orbital character of the resulting MOs contributes significantly to the hyperfine anisotropy. The results suggest that the d_{xy} orbital is depleted of unpaired spin relative to d_{xz} and d_{yz}, which is indicative of a ligand with a substantially different interaction to the other ligands. One such possibility is a histidine ligand. It would provide σ-bonding into a vacant e_g orbital and π-backbonding into the d_{xy} orbital of the metal.

Referring to the anisotropic hyperfine tensor components of Mn^{IV} as A_{xx} etc, it is seen that $A_{yy} \sim -A_{zz}$ and $A_{xx} \sim 0$. If the total squared d orbital components in the relevant MOs are a, b, and c for d_{yz}, d_{xz}, and d_{xy} respectively, the above pattern requires that $b>a>c$ (Appendix IV). That b is largest is totally consistent with the x axis being ligand deficient, as already inferred above from the quadrupole term. The fact that c is smallest would mean that the putative histidine ligand along the y axis is oriented with the p-orbital of the π system parallel to the xy plane (for maximum interaction, see Fig. 5.) Two less strongly π bonding ligands would be located along the z axis.

The above interpretation, in terms of the Mn dimer being coordinatively unsaturated and possessing low symmetry, is tempting since relatively few likely ligands to Mn in the proteins of PSII have been identified. To date, all candidates are on the D1 peptide of the PSII reaction center core. Diner and coworkers, using site-directed mutagenesis, have identified Asp 170, His 190, Tyr 161, His 332, Glu 333, Asp 342, and Ala 344 (carboxy terminal residue) on the D1 protein (Diner et al., 1991; Nixon and Diner, 1992) as important for the assembly of the Mn cluster. Therefore there are three to four possible ligands at present for each Mn dimer, one a histidine. The presence of histidine as a direct ligand to the manganese has been confirmed by electron spin echo envelope modulation experiments (Tang et al., 1994). As the complex accumulates charge during the oxidation cycle, further stabilization of the charge via interaction with π-orbitals would be favorable.

The a_{iso} of −9.4 mT for Mn^{IV} is larger than expected. Factors that may contribute are:

1. Hyperfine constants for an Mn^{IV} ion in a low coordination environment can be very large. Ferrante et al. (1977) recorded the spectra for molecular MnO_2 ($D_{\infty h}$ symmetry) in an argon matrix and found that $A_{\|}$ was 12.5 mT and $A_{\perp}$ was 26.0 mT (Ferrante et al., 1977). This arises from significant unpaired spin density in the metal 4s orbital. The large hyperfine values obtained here may merely be a reflection of an incomplete coordination environment for Mn^{IV} in the protein.

2. The effect of the individual ion crystal field (D) parameters in the strong coupling regime ($D/J \ll 1$) (Zheng et al., 1994) on the effective hyperfine parameters in a Mn^{III}-Mn^{IV} dimer is greater for the Mn^{IV} than for the Mn^{III}. For example, taking $J \sim -50$ cm^{-1}, which is large enough to ensure an isolated ground state, together with typical D values for Mn^{III} of ~ -4 cm^{-1} and for Mn^{IV} of $\sim -1 cm^{-1}$ (Al'tshuler and Kozyrev, 1974), results in effective hyperfine parameters of $A_1 \sim 2.4\, a_1$ and $A_2 \sim -1.4\, a_2$ (Mn^{III} and Mn^{IV}, respectively). These in turn give isolated ion values of $a_{1iso} \sim -7.4$ mT and $a_{2iso} \sim -7.5$ mT. Such values are totally "conventional" (Al'tshuler and Kozyrev, 1974) and caution against using simple arguments based on the multiline pattern width to exlude dimer models. Notwithstanding this, however, the quadrupole interaction indicates an unusual ligand geometry, so that the large a_{iso} is more likely, in our view, to result from a distorted ligand environment, which is further supported by the low (rhombic) symmetry of the hyperfine parameters. Of course some combination of the above effects could be operating.

Linewidth

A change in linewidth was observed with the increase in frequency, indicating that g-strain broadening is important. This is expected due to the slightly larger g-anisotropy seen in PSII compared with model compounds and the manganese catalase, together with the significantly larger hyperfine anisotropy (Haddy et al., 1994; Zheng et al., 1994). It is interesting to note that the increase in linewidth is linear between S- and X-band, but the linearity breaks down at Q-band, where the linewidth is approximately the same as at X-band. This could be due to a contribution of relaxation effects, which are inversely dependent on the applied frequency (the $\omega\tau > 1$ regime).

Although the simulations are, in our judgment, convincing, particularly at X- and Q-bands, they are not yet of the quality achieved for simpler dimer systems, which require hyperfine-only interactions. Of course the multiline pattern is far more complex than any such dimer spectra and the substantial involvement of partially allowed transitions

means that both field positions and intensities must be accurately reproduced. This is particularly challenging at S-band. It is likely that some of the discrepancies observed in the simulations may be indications of non-coincidence of the principal axis directions of the five tensors associated with the two Mn ions. As noted above, this is most evident along the z axis, where the greatest parameter variation with frequency is observed. We suspect that the four hyperfine tensors are probably reasonably well aligned, but that the g-tensor alignment is different from the rest. Exploratory simulations have shown that a coincident z axis, with non-coincident x and y axes of the g-tensor to the hyperfine tensors, does not on its own improve the fit.

Finally, the simulations reported here do not include any orientation dependence or m_I dependence of the linewidth. Although this appears not to be a significant deficiency at X- and Q-bands, it is clear from Fig. 2, *A* and *B* that the intrinsic linewidth at S-band appears to be larger near the pattern edges than in the central region of the spectrum. Further studies incorporating orientation and m_I-dependent linewidth effects are currently in hand.

Model

Fig. 7 shows our current model based on the above results with the relevant coordinate system. The Mn dimer is assumed to be di-μ-oxo, μ-carboxylato bridged to comply with the few ligands known. Model compounds of this configuration have been shown to have Mn-Mn distances of ~2.7 Å (e.g., Christou, 1989). The histidine is pictured as liganded to Mn^{IV} because of the unusual quadrupole interaction and rhombic hyperfine interaction seen at Mn^{IV}. The orientation of the histidine ring plane relative to the cluster is determined by the arguments above. Histidine is an electron-donating ligand, and π-bonding would stabilize oxidation of Mn^{III} to Mn^{IV} in the S_1–S_2 transition. The other ligands are carboxylic acids and presumably substrate water, but both Mn are only 5-coordinate, with the ligand deficient axes determined by the quadrupole terms. Based on model compounds, the axial carboxylic acid oxygen ligands would have longer bonds to Mn (~2.1 Å) than the di-μ-oxo ligands (~1.8 Å) (Bashkin et al., 1987) The histidine with its strong π-interaction would presumably have a shorter bond. A bond length of ~1.9 Å is reported for an imidazole ligand to Mn (Bashkin et al., 1987). These are consistent with the average bond lengths indicated by EXAFS.

CONCLUSIONS

1. The S_2 state multiline signal can be simulated (at three frequencies) using a model consisting of an isolated di-μ-oxo bridged Mn^{III}-Mn^{IV} dimer, antiferromagnetically coupled with net spin ½.

2. For quadrupole interactions of the magnitude indicated here to be present, the Mn^{III} ion must be 5-coordinate, and the Mn^{IV} must also be 5-coordinate, or possibly have a sixth, weakly bound ligand.

3.The hyperfine parameters indicate an anisotropy at Mn^{III} consistent with the Jahn-Teller distortion expected for a d^4 ion, with the unpaired spin in the z direction. The environment at Mn^{IV} is more unusual showing a high degree of anisotropy, not expected in a d^3 ion. This degree of anisotropy can be at least qualitatively accounted for by a histidine providing strong π-backbonding into the d_{xy} orbital, together with a weakly bound or absent ligand in the x direction.

APPENDIX I

The **g** and **A** interactions can be separated into an isotropic, constant component and the anisotropic tensor elements.

The Zeeman terms

$$\beta\mathbf{H}\cdot\mathbf{g}\cdot\mathbf{S} = g_{iso}\beta\,\mathbf{H}\cdot\mathbf{S} + \beta\,\mathbf{H}\cdot\mathbf{g}_{an}\cdot\mathbf{S}$$

The field is taken to be along the z axis and therefore $H_xH_y = 0$. The isotropic term becomes $g_{iso}\beta H_zS_z$. Then

$$\beta\cdot\mathbf{H}\cdot\mathbf{g}_{an}\cdot\mathbf{S} = \beta H_z[g_{zx}S_x + g_{zy}S_y + g_{zz}S_z]$$

and the nuclear Zeeman terms for each Mn: $g_n\beta_nH_zI_z$, where g_n and β_n are the nuclear g-value for Mn and nuclear Bohr magneton. $I_z = 5/2$.

The hyperfine terms

$$\mathbf{S}\cdot\mathbf{A}\cdot\mathbf{I} = A_{iso}\mathbf{S}\cdot\mathbf{I} + \mathbf{S}\cdot\mathbf{A}_{an}\cdot\mathbf{I} = A_{iso}[S_xI_x + S_yI_y + S_zI_z] + S_x[A_{xx}I_x + A_{xy}I_y + A_{xz}I_z] + S_y[A_{yx}I_x + A_{yy}I_y + A_{yz}I_z] + S_z[A_{zx}I_x + A_{zy}I_y + A_{zz}I_z]$$

$S \cdot A \cdot I \cdot$ refers to $S \cdot A_1 \cdot I_1$ or $S \cdot A_2 \cdot I_2$.

The quadrupole terms

$I \cdot Q \cdot I$ refers to $I_1 \cdot Q_1 \cdot I_1$ or $I_2 \cdot Q_2 \cdot I_2$.

$$\mathbf{I}\cdot\mathbf{Q}\cdot\mathbf{I} = Q_{xx}I_x^2 + Q_{yy}I_y^2 + Q_{zz}I_z^2 + Q_{xy}(I_xI_y + I_yI_x) + Q_{xz}(I_xI_z + I_zI_x) + Q_{yz}(I_yI_z + I_zI_y)$$

The complete Hamiltonian in the laboratory frame

Using shift operators: $S_x = 1/2(S_+ + S_-)$ and $S_y = i/2(S_+ - S_-)$ and similarly for I_{1x},I_{1y} and I_{2x},I_{2y} then,

$$\begin{aligned}\mathscr{H} &= g_{iso}\beta H_zS_z + \beta H_z[\tfrac{1}{2}g_{zx}(S_+ + S_-) - \tfrac{1}{2}ig_{yz}(S_+ - S_-) + g_{zz}S_z] \\ &+ g_n\beta_nH_zI_{1z} + A_{1iso}S_zI_z + \tfrac{1}{2}A_{1iso}[S_+I_{1-} + S_-I_{1+}] + \tfrac{1}{4}(A_{1xx} - A_{1yy}) \\ &[S_-I_{1-} + S_+I_{1+}] + \tfrac{1}{4}(A_{1xx} + A_{1yy})[S_-I_{1+} + S_+I_{1-}] \\ &- iA_{1xy}[S_+I_{1+} - S_-I_{1-}] + \tfrac{1}{2}A_{1xz}[S_+ + S_-]I_{1z} \\ &- \tfrac{1}{2}iA_{1yz}[S_+ - S_-]I_{1z} + \tfrac{1}{2}A_{1xz}S_z[I_{1+} + I_{1-}] \\ &- \tfrac{1}{2}iA_{1yz}S_z[I_{1+} - I_{1-}] + A_{1zz}S_zI_{1z} + \tfrac{1}{2}Q_{1zz}[3I_{1z}^2 - I_1^2] \\ &+ \tfrac{1}{4}(Q_{1xx} - Q_{1yy})[I_{1+}^2 + I_{1-}^2] - \tfrac{1}{2}iQ_{1xy}[I_{1+}^2 - I_{1-}^2] \\ &+ \tfrac{1}{2}Q_{1xz}[I_{1+}I_{1z} + I_{1z}I_{1+} + I_{1-}I_{1z} + I_{1z}I_{1-}] - \tfrac{1}{2}iQ_{1yz}[I_{1+}I_{1z} \\ &+ I_{1z}I_{1+} - I_{1-}I_{1z} - I_{1z}I_{1-}]\end{aligned}$$

Here A_1 represents the hyperfine interaction and Q_1 represents the quadrupole interaction at Mn^{III}. I_1 is the nuclear spin for Mn^{III} (5/2) and S is the net electron spin (1/2).

The Hamiltonian is expressed in field space so that all terms are divided by $g_{iso}\beta$ and hence the parameters are expressed in mT.

APPENDIX II

$$\mathbf{R}(\phi,\theta) = \begin{bmatrix} \cos\phi\cos\theta & -\sin\phi & \cos\phi\sin\theta \\ \sin\phi\cos\theta & \cos\phi & \sin\phi\sin\theta \\ -\sin\phi & 0 & \cos\theta \end{bmatrix}$$

Then,

$$A_{1xx} = \cos^2\phi\cos^2\theta X_{1a} + \sin^2\phi\cos^2\theta Y_{1a} - \sin^2\theta(X_{1a} + Y_{1a})$$

$$A_{1yy} = \sin^2\phi X_{1a} + \cos^2\phi Y_{1a}$$

$$A_{1zz} = \cos^2\phi\sin^2\theta X_{1a} + \sin^2\phi\sin^2\theta_1 Y_a - \cos^2\theta(X_{1a} + Y_{1a})$$

$$A_{1xz} = \sin\theta\cos\theta(\cos^2\phi X_{1a} + \sin^2\phi Y_{1a} + X_{1a} + Y_{1a})$$

$$A_{1yz} = \sin\phi\cos\phi\sin\theta(Y_{1a} - X_{1a})$$

$$A_{1xy} = \cos\phi\sin\phi\cos\theta(Y_{1a} - X_{1a})$$

X_{1a} and Y_{1a} are the diagonal components of the traceless tensor where $Z_{1a} = -(X_{1a} + Y_{1a})$. The terms for the other tensors are derived similarly.

APPENDIX III

Generation of random angles in one octant of the unit sphere for calculation of powder pattern spectra (Fig. 8).

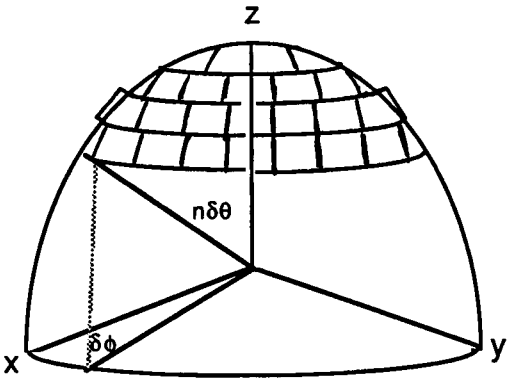

FIGURE 8 Length of arc for an angle increment $\delta\theta$ is $r\,\delta\theta\,(r = 1)$. Length of arc for angle increment $\delta\phi$ is $\delta\phi\,\sin\theta$, which is set equal to $\delta\theta$. For each step n_θ of $\delta\theta$ an approximate square on the surface of the unit sphere is described by $\delta\theta.\delta\phi\sin n_\theta\delta\theta$. Number of tiles ($Nt$) going from x to y axis is given by $Nt = \pi/(2 * \delta\phi)$ (rounded to integer). The offset required to balance the tiles across the octant, OFS = $(\pi/2 - \delta\phi * Nt)/2$. The angle ϕ, for each step of $\delta\theta$, is then given by: OFS + $n_\phi\delta\phi$ as n_ϕ is varied from 1 to Nt. A tile subtending an angle of 4.5°C along an edge results in 284 spectra added together to contribute to the powder pattern.

APPENDIX IV

For each electron in a pure metal $3d$, t_{2g} orbital, the nuclear hyperfine dipole-dipole interaction tensor is given by:

$$A_\parallel = -g_e g_n \beta\beta_n \langle r^{-3}\rangle\, 2/7\mathbf{S} = -2\kappa$$

$$A_\perp = \kappa$$

where S is the total electron spin of the ion (Abragam and Bleaney, 1986, chapter 7). The $_\parallel$ direction is normal to the plane of the orbital lobes, i.e., is the z direction for d_{xy} etc. Assuming $\langle r^{-3}\rangle \sim 5.3$ au^{-3} for Mn^{IV} (Abragam, 1986, chapter 7), κ is ~2.5 mT. Taking a,b, and c as the net fractional components of d_{yz}, d_{xz}, d_{xy} in the MOs carrying unpaired spin density on Mn^{IV}, then

$$A_{xx}/\kappa = -2a + b + c \sim 0$$

$$A_{yy}/\kappa = a - 2b + c \sim -1.4$$

$$A_{zz}/\kappa = a + b - 2c \sim +1.4$$

giving $b - c \sim 0.9$ and $a = 1/2\,(b + c)$

This calculation is only crude, in that it assumes orbital independent free ion values for $\langle r^{-3}\rangle$ among other things, but indicates the $b > a > c$, and that c is relatively small.

We thank Dr L.-E. Andreasson for providing the S-band spectrum, Dr T. Wydrzynski and Dr D. McLachlan for useful discussions, Paul Smith for assistance with EPR spectra, Dr R. Bramley for use of the Q-band EPR spectrometer, and the ANU Supercomputer Facility for use of the vector processor.

REFERENCES

Abragam, A., and B. Bleaney. 1986. Electron Paramagnetic Resonance of Transition Ions. Dover Publications Inc., Mineola, New York.

Al'tshuler, S. A., and B. M. Kozyrev. 1974. Electron Paramagnetic Resonance in Compounds of Transition Elements, 2nd ed. John Wiley & Sons, New York.

Andreasson, L.-E. 1989. Is nitrogen liganded to manganese in the photosynthetic oxygen-evolving system? EPR studies after isotropic replacement with ^{15}N. *Biochim. Biophys. Acta.* 973:465–467.

Bashkin, J. S, H-R. Chang, W. E. Streib, J. C. Huffman, D. N. Hendrickson, and G. Christou. 1987. Modelling the photosynthetic water oxidation center: preparation and physical properties of a tetranuclear oxide bridged Mn complex corresponding to the native S_2 state. *J. Am. Chem. Soc.* 109:6502–6504.

Bonvoisin, J., G. Blondin, J. Girerd, and J. Zimmerman. 1992. Theoretical study of the multiline EPR signal from the S_2 state of the oxygen evolving complex of photosystem II. *Biophys. J.* 61:1076–1086.

Britt, R. D., G. A. Lorigan, K. Sauer, M. P. Klein, and J. Zimmerman. 1992. The g = 2 multiline EPR signal of the S_2 state of the photosynthetic oxygen-evolving complex originates from a ground spin state. *Biochim. Biophys. Acta.* 1040:95–101.

Brudvig, G. W. 1989. EPR spectroscopy of manganese enzymes. *In* Advanced EPR. Applications in Biology and Biochemistry. A. J. Hoff, editor. Elsevier, Amsterdam. 839–863.

Christou, G. 1989. Manganese carboxylate chemistry and its biological relevance. *Acc. Chem. Res.* 22:328–335.

Debus, R. J. 1992. The manganese and calcium ions of photosynthetic oxygen evolution. *Biochim. Biophys. Acta.* 1102:269–352.

DeRose, V. J., I. Mukerji, M. J. Latimer, V. K. Yachandra, K. Sauer, and M. P. Klein. 1994. Comparison of the manganese oxygen-evolving complex in photosystem II of Spinach and *Synechococcus* sp. with multinuclear manganese model compounds by x-ray absorption spectroscopy. *J. Am. Chem. Soc.* 116:5239–5249.

DeRose, V. J., V. K. Yachandra, A. E. McDermott, R. D. Britt, K. Sauer, and M. P. Klein. 1991. Nitrogen ligation to manganese in the photosynthetic oxygen-evolving complex: continuous wave and pulsed EPR studies of photosystem II particles containing ^{14}N or ^{15}N. *Biochemistry.* 30: 1335–1341.

Dexheimer, S. L., and M. P Klein. 1992. Detection of a paramagnetic intermediate in the photosynthetic oxygen-evolving complex. *J. Am. Chem. Soc.* 114:2821–2826.

Diner, B. A., P. J. Nixon, and J. W. Farchaus. 1991. Site-directed mutagenesis of photosynthetic reaction centres. *Curr. Opin. Struct. Biol.* 1:546–554.

Dismukes, G. C., and Y. Siderer. 1981. Intermediates of a polynuclear manganese center involved in photosynthetic oxidation of water. *Proc. Natl. Acad. Sci. USA.* 78:274–278.

Ferrante, R. F., J. L. Wilkerson, W. R. M. Graham, and W. J. Weltner. 1977. ESR spectra of the MnO, MnO_2, MnO_3, MnO_4 molecules at 4° K. *J. Chem. Phys.* 67:5904–5913.

George, G. N., R. C. Prince, and S. P. Cramer. 1989. The manganese site of the photosynthetic water-splitting enzyme. *Science.* 243:789–791.

Goodin, D. B., V. K. Yachandra, R. D. Britt, K. Sauer, and M. P. Klein. 1984. The state of manganese in the photosynthetic apparatus. *Biochim. Biophys. Acta.* 767:209–216.

Haddy, A., R. Aasa, and L.-E. Andreasson. 1989. S-Band EPR studies of the S_2-state multiline signal from the photosynthetic oxygen-evolving complex. *Biochemistry.* 28:6954–6959.

Haddy, A., G. S. Waldo, R. H. Sands, and J. E. Penner-Hahn. 1994. Simulation of multifrequency EPR spectra from Mn(III)/Mn(IV) catalase of *Lactobacillus plantarum* using a new approach based on perturbation theory. *Inorg. Chem.* 33:2677–2682.

Hansson, Ö., and T. Wydrzynski. 1990. Current perceptions of photosystem II. *Photosynth. Res.* 23:131–162.

Hansson, Ö., R. Aasa, and T. Vänngård. 1987. The origin of the multiline and g = 4.1 electron paramagnetic resonance signals from the oxygen-evolving system of photosystem II. *Biophys. J.* 51:825–832.

Hansson, Ö., L.-E. Andreasson, and T. Vänngård. 1986. Oxygen from water is coordinated to manganese in the S_2 state of photosystem II. *FEBS Lett.* 195:151–154.

Kessissoglou, D. P., M. L. Kirk, C. A. Bender, M. S. Lah, and V. L. Pecoraro. 1989. A bent mixed-valence manganese (III/II/III) complex: a new class of trinuclear, acetate bridged Schiff's base compounds exhibiting a g = 2 multiline ESR signal. *J. Chem. Soc. Chem. Commun.* 84–86.

Kok, B., B. Forbush, and M. McGloin. 1970. Cooperation of charges in photosynthetic O_2 evolution-1: a linear four step mechanism. *Photochem. Photobiol.* 11:457–475.

Kusonoki, M. 1992. A new paramagnetic hyperfine structure effect in manganese tetramers. The origin of the 'multiline' EPR signals from an S_2 state of a photosynthetic water-splitting enzyme. *Chem. Phys. Lett.* 197: 108–116.

Landolt-Börnstein, 1988. Numerical Data and Functional Relationships in Science and Technology, Group III, Vol 20a. K. H. Hellwege and A. M. Hellwege, editors. Springer-Verlag, Berlin.

Liang, W., M. J. Latimer, H. Dau, T. A. Roelofs, V. K. Yachandra, K. Sauer, and M. P. Klein. 1994. Correlation between structure and magnetic spin state of the manganese cluster in the oxygen-evolving complex of photosystem II in the S_2 state: determination by x-ray absorption spectroscopy. *Biochemistry.* 33:4923–4932.

Lorigan, G. A, and R. D. Britt. 1994. Temperature-dependent pulsed electron paramagnetic resonance studies of the S_2 state multiline signal of the photosynthetic oxygen-evolving complex. *Biochemistry.* 33: 12072–12076.

MacLachlan, D. J., B. J. Hallahan, S. V. Ruffle, J. H. A. Nugent, M. C. W. Evans, R. W. Strange, and S. S. Hasnain. 1992. An EXAFS study of the manganese O_2-evolving complex in purified photosystem II membrane fractions. *Biochem. J.* 285:569–576.

Nixon, P. J., and B. A. Diner. 1992. Aspartate 170 of the photosystem II reaction center polypeptide D1 is involved in the assembly of the oxygen-evolving manganese cluster. *Biochemistry.* 31:942–948

Pace, R. J., P. Smith, R. Bramley, and D. Stehlik. 1991. EPR saturation and temperature dependence studies on signals from the oxygen-evolving centre of photosystem II. *Biochim. Biophys. Acta.* 1058:161–170.

Penner-Hahn, J. E., R. M. Fronko, V. L. Pecoraro, C. F. Yocum, S. D. Betts, and N. R. Bowlby. 1990. Structural characterization of the manganese sites in the photosynthetic oxygen-evolving complex using x-ray absorption spectroscopy. *J. Am. Chem. Soc.* 112:2549–2557.

Press, W. H., S. A. Teukolsky, W. T. Vetterling, and B. P. Flannery. 1986. Numerical recipes in fortran: the art of scientific computing. Cambridge University Press, Cambridge, UK.

Rutherford, A. W. 1985. Orientation of EPR signals arising from components in photosystem II membranes. *Biochim. Biophys. Acta.* 807:189–201.

Sands, R. H., and W. R. Dunham. 1975. *Q. Rev. Biophys.* 7:443.

Sarneski, J. E., H. H. Thorp, G. W. Brudvig, R. H. Crabtree, and G. K. Schulte. 1990. Assembly of high-valent oxomanganese clusters in aqueous solution. Redox equilibrium of water stable $Mn_3O_4^{4+}$ and $Mn_2O_2^{3+}$ complexes. *J. Am. Chem. Soc.* 112:7255–7260.

Schmitt, E. A., L. Noodleman, E. J. Baerends, and D. N. Hendrickson. 1992. LCAO Xα calculation of the magnetic exchange interactions in a Mn^{IV} and Mn^{III}_3 cubane complex: relevance to the water oxidation center of photosystem II. *J. Am. Chem. Soc.* 114:6109–6119.

Slichter, C. P. 1978. Principles of Magnetic Resonance. Springer-Verlag, Berlin.

Smith, P. J., K. A. Åhrling, and R. J. Pace. 1993. Nature of the S_2 state electron paramagnetic resonance signals from the oxygen evolving complex of photosystem II: Q-band and oriented X-band studies. *J. Chem. Soc. Faraday Trans.* 89:2863–2868.

Tang, X.-S., B. A. Diner, B. S. Larsen, M. L. Gilchrist, Jr., G. A. Lorigan, and R. D. Britt. 1994. Identification of histidine at the catalytic site of the photosynthetic oxygen-evolving complex. *Proc. Natl. Acad. Sci. USA.* 91:704–708.

Yachandra, V. K., V. J. DeRose, M. J. Latimer, I. Mukerji, K. Sauer, and M. P. Klein. 1993. Where plants make oxygen: a structural model for the photosynthetic oxygen-evolving manganese cluster. *Science.* 260: 675–679.

Yachandra, V. K., R. D. Guiles, A. E. McDermott, J. L. Cole, R. D. Britt, S. L. Dexheimer, K. Sauer, and M. P. Klein. 1987. Comparison of the structure of the manganese complex in the S_1 and S_2 states of the photosynthetic O_2-evolving complex: an x-ray absorption spectroscopy study. *Biochemistry.* 26:5974–5981.

Yachandra, V. K., R. D. Guiles, K. Sauer, and M. P. Klein. 1986. The state of manganese in the photosynthetic apparatus. 5. The chloride effect in photosynthetic oxygen evolution. *Biochim. Biophys. Acta.* 850:333–342.

Zheng, M., and G. C. Dismukes. 1992. Photosynthetic water oxidation: what have we learned from the multiline EPR signals? *In* Research in Photosynthesis, Vol. II. N. Murata, editor. Kluwer Academic Publishers, The Netherlands. 305–308.

Zheng, M., S. V. Khangulov, G. C. Dismukes, and V. V. Barnynin. 1994. Electronic structure of dimanganese(II, III) and dimanganese(III, IV) complexes and dimanganese catalase enzyme: a general EPR spectral simulation approach. *Inorg. Chem.* 33:382–387.